Multifunctional Nanocomposites with Reduced Viscosity

Anish Tuteja,[†] Phillip M. Duxbury,[‡] and Michael E. Mackay*[,†,‡]

Department of Chemical Engineering and Materials Science and Department of Physics and Astronomy, Michigan State University, East Lansing, Michigan 48824

Received June 13, 2007; Revised Manuscript Received October 11, 2007

ABSTRACT: It is demonstrated that nanocomposites exhibiting reduced viscosity and multifunctional performance enhancements may be fabricated using simple processing procedures. These behaviors are elucidated by analysis of the effects of dispersed organic (fullerene) nanoparticles and inorganic (magnetite) nanoparticles on the behavior of polystyrene, demonstrating that simple spherical nanoparticles can induce a range of unexpected behavior due to nanoscale effects. In general, multifunctional performance improvements including enhanced mechanical, electrical, magnetic and thermal degradation properties as well as reduced viscosity are promoted when simple design guidelines are followed. These guidelines are tabulated.

1. Introduction

Nanomaterials fabricated by dispersing nanoparticles in polymer melts have the potential for performance that far exceeds that of traditional composites. Though property improvements have been achieved in a variety of nanocomposites,[1−3] nanoparticle dispersion is difficult to control, with both thermodynamic and kinetic processes playing significant roles. Moreover, the addition of anisotropic nanoparticles to polymer melts results in increased viscosity, which may induce processing difficulties. Recently, we demonstrated strategies for the dispersion of isotropic organic nanoparticles in polymers by controlling both thermodynamics and kinetics, and we showed that the viscosity of these materials is decreased, increasing processability.[4−6] Here we provide details of the processing methods used, and more importantly, we show that nanocomposites fabricated in this manner may exhibit multifunctional behavior. We illustrate our methods by studying the effect of dispersed organic (fullerene) nanoparticles and inorganic (magnetite) nanoparticles on the behavior of polystyrene, demonstrating that simple spherical nanoparticles can induce a range of unexpected multifunctional behavior through nanoscale phenomena.

Previously, we demonstrated that dispersed polymer nanoparticles reduce the viscosity of polymer melts[5] and that nanoparticle dispersion is enhanced when the radius of gyration of the melt chains is greater than the nanoparticle radius.[4] In this study we demonstrate that dispersed spherical nanoparticles can yield a range of multifunctional behavior, including a viscosity decrease, reduction of thermal degradation, increased mechanical damping, and enriched electrical and/or magnetic performance. These behaviors are illustrated using two simple examples: unfunctionalized fullerenes (C_{60}) and organically functionalized magnetite nanoparticles in polystyrene melts.

We show that dispersion is essential to multifunctionality through a range of characterization studies assessing the effect of rapid precipitation (RP) methods, as compared to more conventional solvent evaporation (SE), on the state of fullerene dispersion. Well-dispersed fullerene nanocomposites exhibit a remarkable order of magnitude reduction in viscosity as well as improved thermal degradation resistance and mechanical damping. Rapid precipitation also enables efficient dispersion of functionalized magnetic nanoparticles which are characterized using TEM and which yield reduced viscosity materials that are magnetically active. Moreover, these nanoparticles also reduce thermal degradation of polystyrene.

Recently, fullerenes (C_{60} or bucky balls, diameter ~0.7 nm) have garnered widespread attention as nanofillers, with pure fullerenes and their derivatives being used to impart fascinating photonic, electronic, and biomedical properties, which could prove useful for a gamut of future applications, including solar cells,[7,8] superconductive materials,[9,10] and drug delivery.[11] However, dispersion of fullerenes in polymer melts has proven quite difficult.[12−14] To improve the compatibility of fullerenes with bulk polymers, various techniques, including the modification of fullerene structure and direct attachment of fullerenes to the polymer backbone by covalent bonds, have been tried. These methods, apart from being resource intensive, are still unable to produce fully dispersed blends.[15]

In our previous work,[4] we showed that when the polymer radius of gyration (R_g) is greater than the nanoparticle radius (a), nanoparticle dispersion may be enhanced. It appears as if R_g of the polymer increases in the blend, signaling a less favorable dispersed state, yet others have found mixed behavior; i.e., it increases or decreases[16,17] or remains constant.[18] Clearly, polymer swelling, as well as the state of dispersion, is dependent on the details of the system. For example, our hypothesis[4] is that if the nanoparticles are large enough, say 5−10 nm in diameter, then the interstices between them are large enough such that the van der Waals forces cannot effectively propagate across the gap. If the nanoparticles are dispersed in the polymer melt, then they gain molecular contacts on all of their surface, and so a favorable mixing enthalpy is expected. This is indeed what we found when polystyrene nanoparticles were blended with linear polystyrene; a negative χ parameter was obtained.

If the nanoparticle is small, such as for a C_{60} fullerene, then there is little of this mixing enthalpy present, and so dispersion is promoted by enhanced interaction at the monomer−monomer level. Dispersion in the case of fullerenes is promoted merely by the mixing entropy term as we have discussed previously.[4] However, for larger nanoparticles it is expected that the mixing enthalpy discussed above is present, and so the R_g increase, which is entropically unfavorable, is tolerated because of this to create a homogeneous blend. The nanoparticles essentially

* Corresponding author: e-mail mackay@msu.edu, Tel +517-432-4495.
[†] Department of Chemical Engineering and Materials Science.
[‡] Department of Physics and Astronomy.

10.1021/ma071313i CCC: $37.00
Published on Web 11/17/2007

behave as a solvent, a *solid solvent*, to promote mixing. One should also read recent theoretical efforts in this area.[19−22]

However, even when the dispersed state is thermodynamically stable, it may be inaccessible unless the correct processing method is employed. We found that rapid precipitation can be used to produce miscible fullerene−polystyrene nanocomposites up to a maximum concentration of ∼2 vol % in linear, monodisperse polystyrene, as have others with carbon nanotube systems.[23] In comparison, gradual solvent evaporation, a method typically employed for nanoparticle dispersion, leads to large-scale phase separation of the fullerenes. The thermal stability of the dispersed state is confirmed by long time annealing studies which produced no aggregation of the fullerenes.

Despite success in dispersing some simple nanoparticles in polymer melts, the majority of inorganic nanoparticles require organic functionalization in order for stable dispersion to be achieved. Recent work[24] has provided guidance as to the graft density and chain length of the organic layers required to promote thermodynamically stable dispersion, though the correct processing method is still required. In this contribution, we show that the nanoparticle dispersion methods we have developed provide a facile route to dispersion of functionalized nanoparticles, and we demonstrate the utility of the approach by fabricating multifunctional magnetic nanocomposites.

2. Experimental Methods

Materials Used. The fullerenes (C_{60}) were obtained from Sigma-Aldrich (∼98% pure, catalog no. 483036) while the magnetite (Fe_3O_4) nanoparticles were obtained from the Ferrotec Corp. (catalog no. EMG 1400). These particles are coated with a stabilizing dispersing agent (oleic acid) to enable their solubility in organic solvents (the particles may contain up to 20 wt % oleic acid, as specified by the manufacturer). Polystyrene was ordered from Scientific Polymer Products (catalog no. 686) and had a weight-average molecular mass of 393 kDa with a polydispersity index of 1.16.

Rapid Precipitation (RP) Method. Fullerenes were dissolved in toluene at a concentration of 2 mg/mL, while the magnetite nanoparticles were dissolved in benzene at a concentration of 1 mg/mL (as the particles are paramagnetic, the solutions are easily prepared by leaving the magnetite−benzene solution on a magnetic stir plate, without any stir bar). Next, an appropriate amount of polystyrene was added to each solution based on the desired weight fractions of polystyrene and nanoparticles in the final nanocomposite. The solutions were then added dropwise into a large volume of methanol (the solution is continuously stirred using a magnetic stir bar) to enable coprecipitation of polystyrene and the nanoparticles (∼10 mL of methanol is used for every 1 mL of solution). The solids were filtered from methanol and dried in vacuum at 50 °C for at least a week to ensure complete solvent removal. An important background test was to confirm that the surfactant on the magnetite particles was not removed from the magnetite particles during the precipitation process. For this, magnetite particles were dissolved in benzene at a concentration of 1 mg/mL. This solution was then added dropwise to a large volume of constantly stirred methanol (∼10 mL of methanol is used for the precipitation for every 1 mL of solution). The methanol−benzene mixture was then removed by filtration and vacuum drying. The remaining precipitate was found to be almost completely soluble in benzene, confirming that most of the surfactant was not removed during the RP method.

Solvent Evaporation (SE) Method. Fullerenes and polystyrene were codissolved in toluene, while the magnetite particles and polystyrene were codissolved in benzene, using the same methods and concentrations as those for the RP method. This was followed by casting the polymer−nanoparticle solution onto a glass slide. The samples were then left to dry at room temperature for 3 days, followed by drying under vacuum at 50 °C for a week.

Rheological Measurements. For rheological measurements, the solids obtained after the rapid precipitation process were pressed in to 8 mm diameter discs, under vacuum, in a specially designed pellet press. These discs were used with the 8 mm parallel plates fixture of a Rheometrics ARES rheometer set at a gap of ∼0.4 mm and under a nitrogen atmosphere. Frequency sweeps in the range 0.1−100 rad/s were performed at various temperatures (between 130 and 210 °C) and then combined using time−temperature superposition to yield a master curve at 170 °C. The strain during the dynamic shear test was kept small enough to ensure that all response was in the linear viscoelastic region. Further, to check for thermal degradation, after the completion of the test, the highest temperature (210°C) was maintained for 20 min, and the frequency sweep was repeated. The data between the two frequency sweeps matched well for all samples. Also, as will be described below, the addition of nanoparticles to the polymer improves the thermal stability of the nanocomposites, further ensuring that the samples are not thermally degraded during our rheological testing. Furthermore, although not done as part of this study, we have taken samples following rheological testing and used static light scattering to confirm there was no significant (that we could measure) degradation of the linear polymer.

Films for Dynamic Mechanical Analysis (DMA). The disks obtained from the pellet press were also used to make films by compression in a Wabash compression molding press at 160 °C. Steel spacers were used to obtain the desired film thickness. After compression the films were aged at 170 °C for 3−4 h to ensure homogeneity, and then samples were cut from the film for dynamic mechanical analysis with a Rheometrics RSA III. These films were also used as samples for wide-angle X-ray diffraction and electrical conductivity tests.

Differential Scanning Calorimetry (DSC) and Thermogravimetric Analysis (TGA). Thermal analysis was performed using a TA Instruments Q1000 DSC. Samples were heated and cooled at 5 °C/min. Thermogravimetric analysis (TGA) was carried out using a TA Instruments Q50 TGA. Here, the samples were heated at 20 °C/min from room temperature to 330 °C and held isothermally for up to 24 h.

Electrical Conductivity Measurements. The electrical conductivity measurements were performed on a Gamry reference 600 potentiostat, while the obtained data were analyzed using the EIS300 software. The instrument measured the electrical impedance (both the resistance and reactance were obtained for each sample) for various samples, at room temperature, at frequencies varying between 0.1 Hz and 100 kHz (data were collected at 10 different frequencies per decade). The area and thickness for each sample were also measured to enable the calculation of resistivity as a function of frequency from the measured impedance.

3. Results and Discussion: Fullerene−Polystyrene Nanocomposites

In Figure 1, we compare nanocomposites produced by gradual solvent evaporation (SE) with those fabricated using rapid precipitation (RP). The formation of phase-separated structures in SE materials, evident in Figure 1a, is due to the lower solubility of fullerenes as compared to the linear polymer so that slow evaporation of the solvent causes the fullerenes to precipitate from solution before the linear polymer, leading to large fullerene-rich aggregates. However, in the RP method the nanoparticles and linear polymer separate out of solution together, enabling formation of dispersed polymer−nanoparticle blends.[5,23] Long time annealing of RP materials yields no change in their state of dispersion, demonstrating their thermal stability. Moreover, RP nanocomposites can be drawn into fibers (Figure 1b), and no large-scale aggregates are apparent. They can also be compression-molded to form thin films, as illustrated in Figure 1c,d.

Clear evidence of the greater segregation of SE materials is provided in Figure 2a where wide-angle X-ray scattering

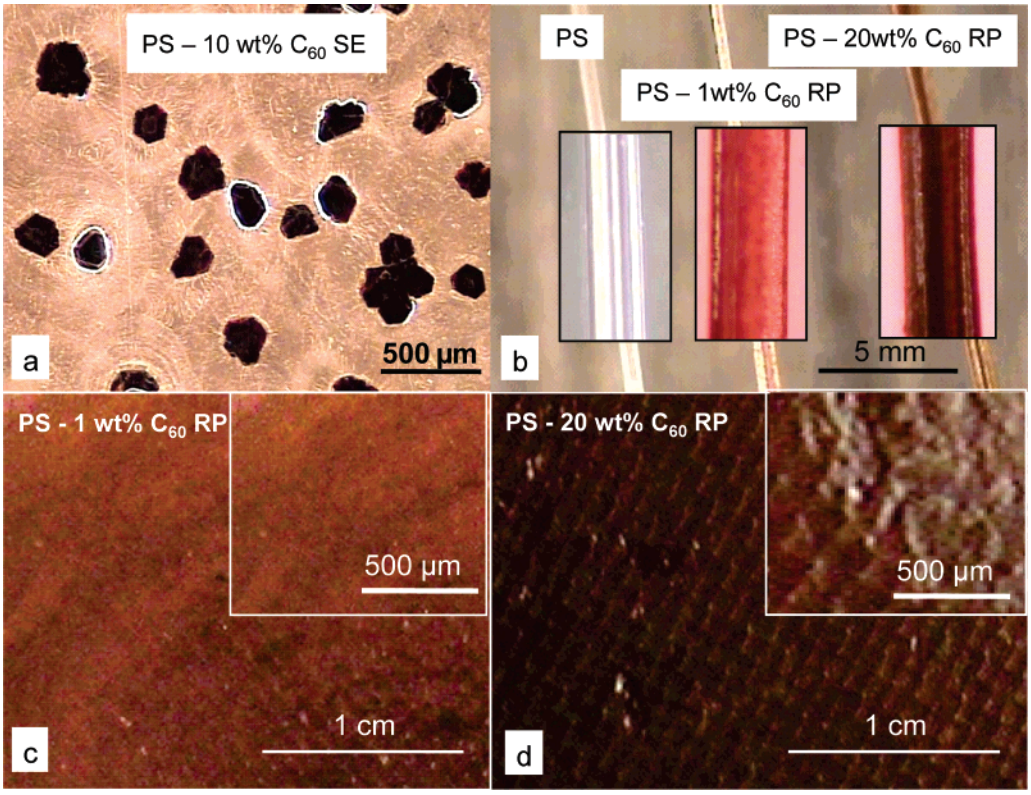

Figure 1. Fullerene dispersion in monodisperse linear polystyrene by rapid precipitation as compared to solvent evaporation. (a) Fullerene (C_{60})−polystyrene (PS) mixtures fabricated by solvent evaporation (SE) produce large phase-separated domains (PS−10 wt % C_{60} SE). (b) Rapid precipitation (RP) yields more homogeneous blends that allow melt spinning of fibers of pure polystyrene (PS), PS with 1 wt % fullerenes (PS−1 wt % C_{60} RP), and PS with 20 wt % fullerenes (PS−20 wt % C_{60} RP). The RP nanocomposites can also be compression molded to prepare free-standing, thin films as shown in the optical micrographs (c) and (d). Markings on the films are from the platens used for compression molding. In all cases the polystyrene has a molecular weight of 393 kDa.

(WAXS) intensity data are plotted as a function of the scattering wave vector ($q = 4\pi/\lambda \sin(\theta/2)$, where λ is the X-ray wavelength (1.54 Å) and θ the scattering angle). It can be seen that the blend prepared by SE displays a large degree of low q scattering, indicating large-scale phase separation,[25] which is absent in the blends prepared by RP. TEM experiments verified the greater segregation in the SE blends and also identified small phase-segregated regions, approximately 200−300 nm in size (Figure 2b), for RP materials at higher fullerene concentrations. RP materials at 1 wt % concentration showed no evidence of these phase-segregated regions. To ensure stable nanostructures, all of the samples were annealed for ∼24 h at 170 °C, which is above the glass transition temperature of polystyrene (106 °C), before performing the TEM and WAXS experiments.

In Figure 2c, we show the WAXS intensity as a function of d spacing for RP nanocomposites at various fullerene concentrations. Here $d = 2\pi/q$, and no sharp peaks are present in the WAXS intensity profile for the 1 wt % nanocomposite, confirming the absence of phase-separated fullerene domains at low fullerene concentrations;[26] moreover, at higher concentrations, peaks in the WAXS intensity emerge. These match well with those seen for fullerene single crystals,[27] as shown in the figure, and are the result of scattering from phase-separated crystallites in the higher concentration blends.

To further characterize the fullerene phase-segregated regions, electron diffraction patterns at different temperatures were collected from fullerene crystallites produced by SE (Figure 2d,e). The diffraction pattern for the fullerene crystallites produced by SE at room temperature (Figure 2d) has hexagonal symmetry, indicating a face-centered-cubic crystal structure. There is a change in the diffraction pattern and hence the crystal structure on lowering the temperature to −50 °C (Figure 2e), which can be related to a transition from face-centered-cubic packing to simple cubic as occurs in pure fullerene materials. The much smaller crystallites present in the 5 and 10 wt % samples produced by RP also showed a diffraction pattern with hexagonal symmetry at room temperature (similar to Figure 2d); however, no change in structure was observed in the diffraction pattern on lowering the temperature to −70 °C[28] (which was the limit of temperature control in the TEM).

Further evidence of this effect is provided by differential scanning calorimetry (DSC) measurements presented in Figure 2f, where we observe a first-order transition from a simple cubic to face-centered-cubic structure at around −15 °C for pure fullerenes and also for phase-segregated regions in SE materials.[27] However, 10 wt % RP nanocomposites show no indication of the pure fullerene crystal transition. The glass transition for polystyrene is also apparent at ∼105 °C in Figure 2f. This provides further evidence that fullerene segregation in SE materials is well developed due to precipitation and growth of pure fullerene clusters during the slow evaporation process.

A notable aspect of nanocomposites is the size of the average interparticle half-gap (h) approximated by $h/a = [\phi_m/\phi]^{1/3} - 1$, where ϕ_m is the maximum random packing volume fraction (∼0.638). At a fullerene weight fraction of 0.01, the average interparticle half-gap is only about 1.3 nm, which is much smaller than the radius of gyration (R_g) (∼17 nm) of the polystyrene, with molecular weight 393 kDa, used to produce the results of Figure 1.[29] Clearly, in the dispersed state, the linear polymer must be distorted from its equilibrium conformation because of the presence of dispersed fullerenes.[6] Higher particle loadings are expected to further enhance this distortion, and the

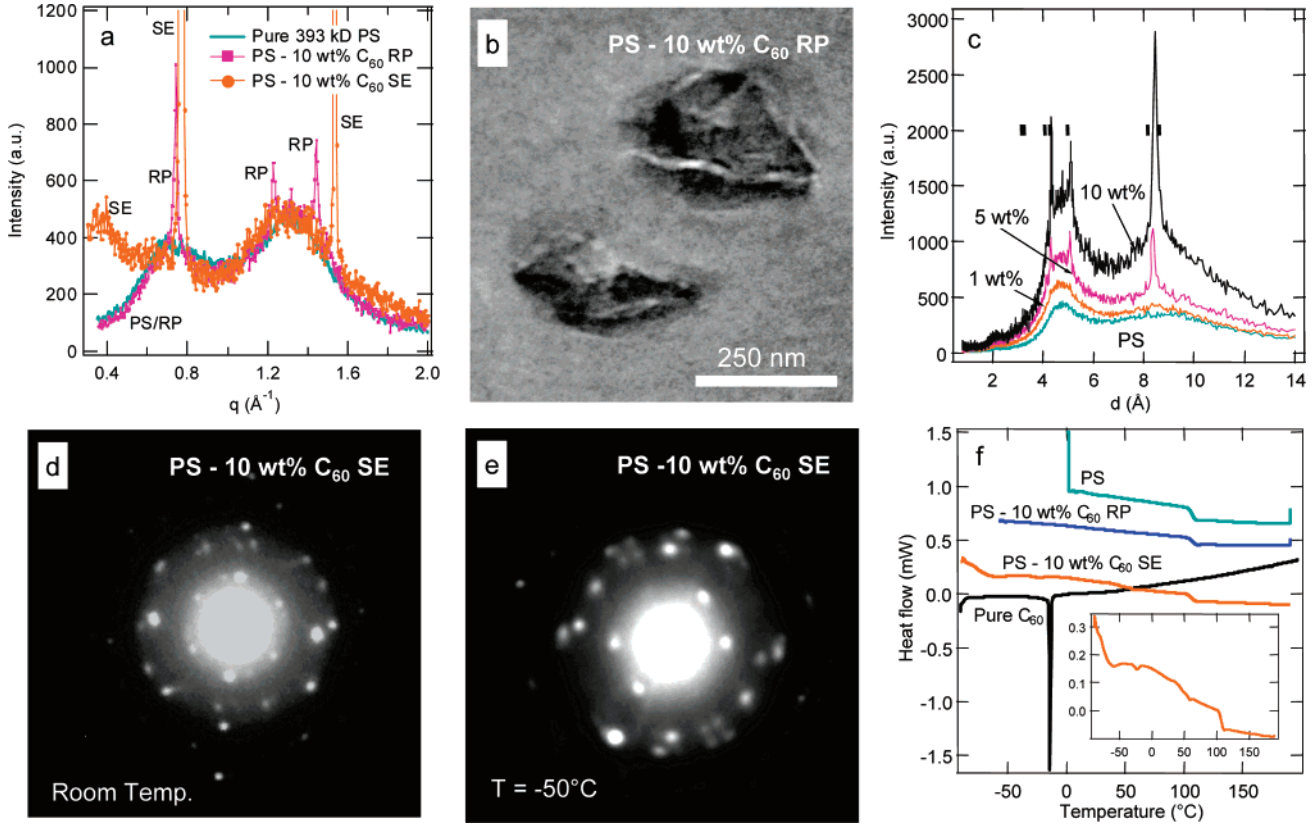

Figure 2. Characterization of fullerene−polystyrene blends. (a) The WAXS intensity profiles, as a function of wave vector (q), for 10 wt % fullerene−polystyrene mixtures produced via rapid precipitation (PS−10 wt % C_{60} RP) and solvent evaporation (PS−10 wt % C_{60} SE) are vastly different with the latter showing low q scattering, indicative of large-scale phase separation. The data for the sample prepared by rapid precipitation agrees well with that for pure polystyrene (PS) at low q vector. Peaks are labeled according to RP, SE, and PS to help discern their origin. (b) A TEM micrograph for the 10 wt % fullerene mixture produced by rapid precipitation shows some phase-separated crystallites which obviously contribute to the WAXS spectrum in (a). (c) The change in the polystyrene WAXS intensity profile (PS) with addition of fullerenes for mixtures produced with rapid precipitation can be significant. At 5 and 10 wt % fullerenes (5 and 10 wt %) evidence of a crystalline structure becomes clear; while the amorphous halo for polystyrene is only slightly changed through addition of 1 wt % fullerenes (1 wt %). The lines at an intensity of 2000 are positions of the structure peaks seen for a fullerene single crystal plotted as a function of d-spacing. (d) An electron diffraction pattern from a crystallite present in a blend prepared by solvent evaporation at room temperature demonstrating 6-fold symmetry. (e) Electron diffraction pattern from another crystallite, within the same sample, at −50 °C. The diffraction pattern changes from 6-fold to 4-fold symmetry when the temperature is lowered, while no such symmetry change was found with the samples prepared via rapid precipitation. (f) Differential scanning calorimetry (DSC) results to show dispersion of 10 wt % fullerenes (C_{60}) in 393 kDa polystyrene (PS) via rapid precipitation (RP) leads to a single glass transition of the nanocomposite (PS−10 wt % C_{60} RP), with a glass transition that is slightly greater than that for pure 393 kDa polystyrene (PS). Pure fullerenes have a crystal structure transition around −15 °C (pure C_{60}) which is absent in the nanocomposite produced by rapid precipitation but is present in the phase-separated film produced by solvent evaporation (PS−10 wt % C_{60} SE), as can be seen more clearly in the inset.

interparticle gap decreases to about 0.4 nm at a fullerene weight fraction of 0.1. At this weight fraction, the interparticle gap is comparable to the fullerene equilibrium separation in a single crystal[27] and also the polystyrene monomer size. It is thus surprising that fullerene dispersion is possible up to volume fractions of order 1 vol %.

A rough estimate of the ultimate solubility of fullerenes in polymers can be made using Flory theory[4,30] to arrive at the particle binodal volume fraction (ϕ_B) of $-\ln(\phi_B) \approx 1 + \chi$ in the limit of small nanoparticle concentration. The χ parameter is related to the molecular insertion energy on a lattice (ϵ) and given by $\chi = z\epsilon/k_BT$, where z is the coordination number, k_B the Boltzmann constant, and T the temperature. Even if χ is positive and opposes dispersion, the large mixing entropy due to the small size of fullerenes means that even with positive χ values of order 1−10, stable dispersions of up to ∼10 vol % are theoretically possible. Liquid state theory (PRISM) calculations[21] suggest a miscibility window depending on the interaction energy between the polymer and the nanoparticle as compared to the other interaction energies in the problem, and earlier calculations on clay materials demonstrate the requirement of a negative effective χ for their thermodynamically stable dispersion.[31,32] In general, if the insertion energy is sufficiently negative (favorable), dispersion will occur for any nanoparticle size or shape; however, the entropic cost of distorting the polymer chains must be overcome for this to occur, a balance which is achieved more readily when spherical nanoparticles are smaller than the polymer radius of gyration.[4]

In our previous work,[5] we reported for the first time that the addition of intramolecularly cross-linked polystyrene nanoparticles to linear polystyrene causes a *decrease* in the polymer melt viscosity, contradicting Einstein's century old relation. It was postulated that the viscosity decrease observed in these nanocomposites was directly related to the increase in the melt free volume caused by nanoparticle addition.[33] However, subsequent experiments[6] revealed that a change in free volume does not account for all of the effects observed in this system, with a viscosity decrease only present for entangled and confined ($h < R_g$) systems. Indeed, addition of nanoparticles led to a viscosity increase in unentangled polymers. This provides two design parameters to cause a viscosity *reduction* in nanocomposites: the polymer must be entangled ($M > M_c$, where M_c is the critical molecular mass critical mass for entanglement coupling[34]), and the interparticle half-gap must be less than the

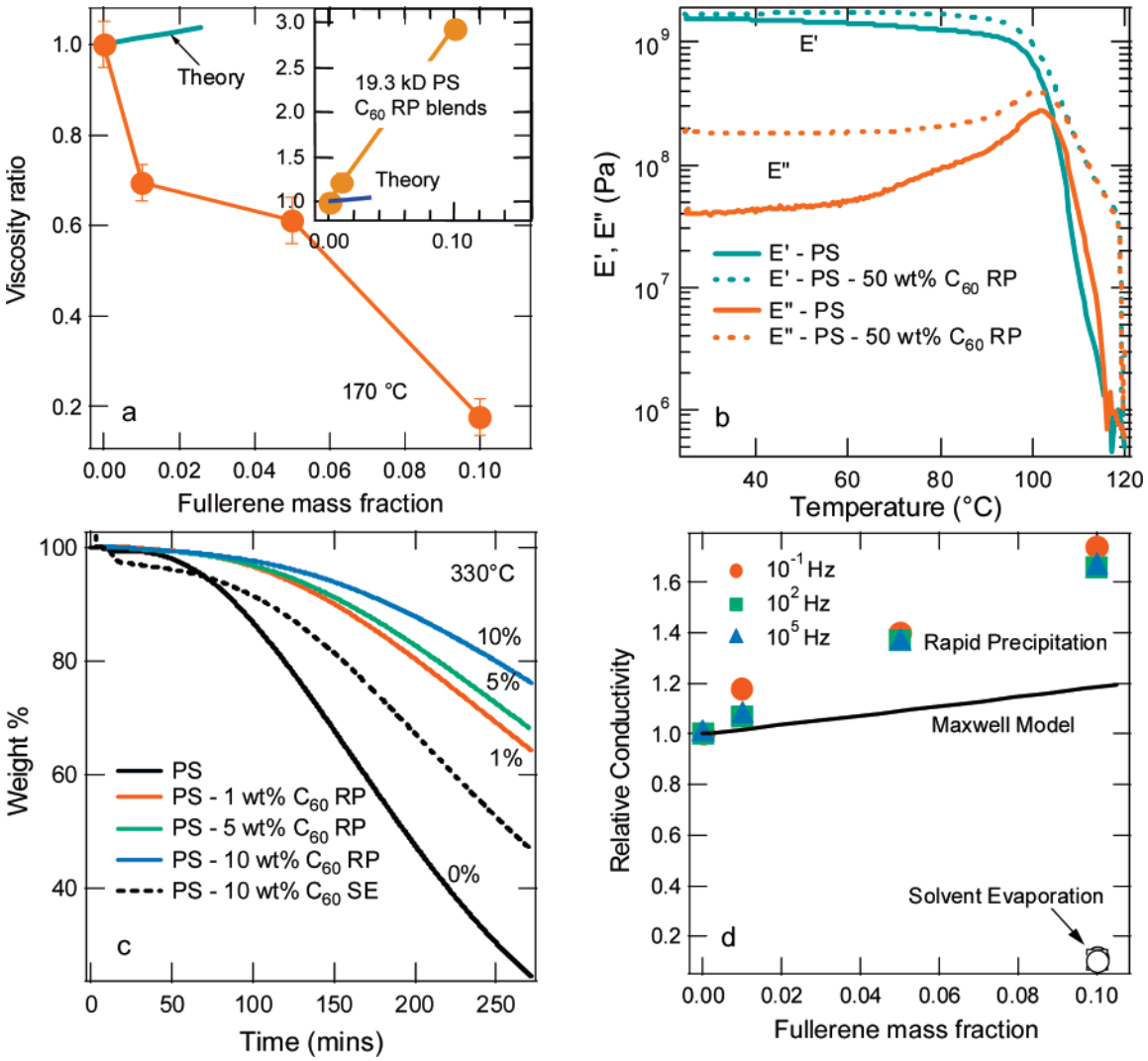

Figure 3. Multifunctional properties of fullerene−polymer nanocomposites. (a) The addition of fullerenes to polystyrene leads to a sharp decrease in the melt viscosity as long as the samples are prepared by rapid precipitation. The inset shows the effect of fullerene addition on the viscosity of unentangled polystyrene (M_w = 19.3 kDa) where a large viscosity increase is evident. The line labeled "Theory" is Einstein's prediction. (b) Minimal changes are seen in the storage (E') modulus on the addition of fullerenes while a 5-fold increase is observed in the loss (E'') modulus, indicating a significant improvement in the damping properties of the composite. The samples shown in the figure are for pure 393 kDa polystyrene (PS) and the same molecular weight polystyrene containing 50 wt % fullerenes produced by rapid precipitation. (c) The addition of fullerenes, when well dispersed, greatly reduces the rate of thermal decomposition of the nanocomposite as shown by weight loss curves obtained by heating the samples to 330 °C, under a nitrogen atmosphere. The samples containing 1−10 wt % C_{60}, produced by rapid precipitation (solid curves, PS−1 wt % C_{60} RP, etc.), when compared to pure 393 kDa polystyrene (PS), have a much lower degradation rate. In comparison, phase-separated fullerenes perform much worse, and a 10 wt % blend prepared by solvent evaporation (dashed curve, PS−10 wt % C_{60} SE) only slightly reduces the degradation rate. (d) When various concentration fullerenes are dispersed in polystyrene, using rapid precipitation, the electrical conductivity rises above the Maxwell model prediction for an infinitely conducting particle. In comparison, a sample containing phase-separated structures, produced by solvent evaporation, has a relative conductivity that is ∼90% lower than pure polystyrene. Conductivity was measured at a variety of frequencies, and only the values obtained at 10^{-1}, 10^2, and 10^5 Hz are shown.

polymer size ($h < R_g$). It should also be pointed out that the shape of the nanoparticles is extremely important since only spherical nanoparticles have been shown to provide a viscosity decrease so far, with other nanofillers like nanoclays[35] and carbon nanotubes[36,37] producing a large increase in the viscosity of the polymer melt, leading to more challenging processing conditions.

From Figure 3a it can be seen that the unusual viscosity decrease first seen in the ideal polystyrene nanoparticle−linear polystyrene system also occurs in fullerene−polystyrene systems formed by RP, provided the polymer melt is entangled. Moreover, the viscosity decreases with increasing fullerene concentrations for the PS 393 kDa system, which is entangled with R_g = 17 nm, so that $R_g > a$ (note for all nanoparticle concentrations considered here $h < R_g$). Indeed, an 80% reduction in the melt viscosity can be observed in the 10 wt % fullerene RP materials, which is one of the largest reductions in polymer viscosity, on the addition of nanoparticles, reported in the literature. As noted above in the characterization studies, phase-separated fullerene structures (crystallites) are present in the 5 and 10 wt % RP samples (Figure 2), so it is interesting that the viscosity continues to decrease even in the presence of these crystallites. In contrast, the 10 wt % fullerene SE system showed a large viscosity increase above that of pure polystyrene, and no terminal (zero shear rate) viscosity was apparent. The larger aggregates occurring in SE materials clearly offset the nanoscale phenomena leading to viscosity reduction seen in RP materials. Moreover, because of the gradual color change in the RP nanocomposites (see Figure 1c), we suspect there may be more fullerenes dissolved in the polystyrene-rich phase for the 10 wt % RP blend than at the initial concentration where phase separation was detected (∼2 vol %). This may account

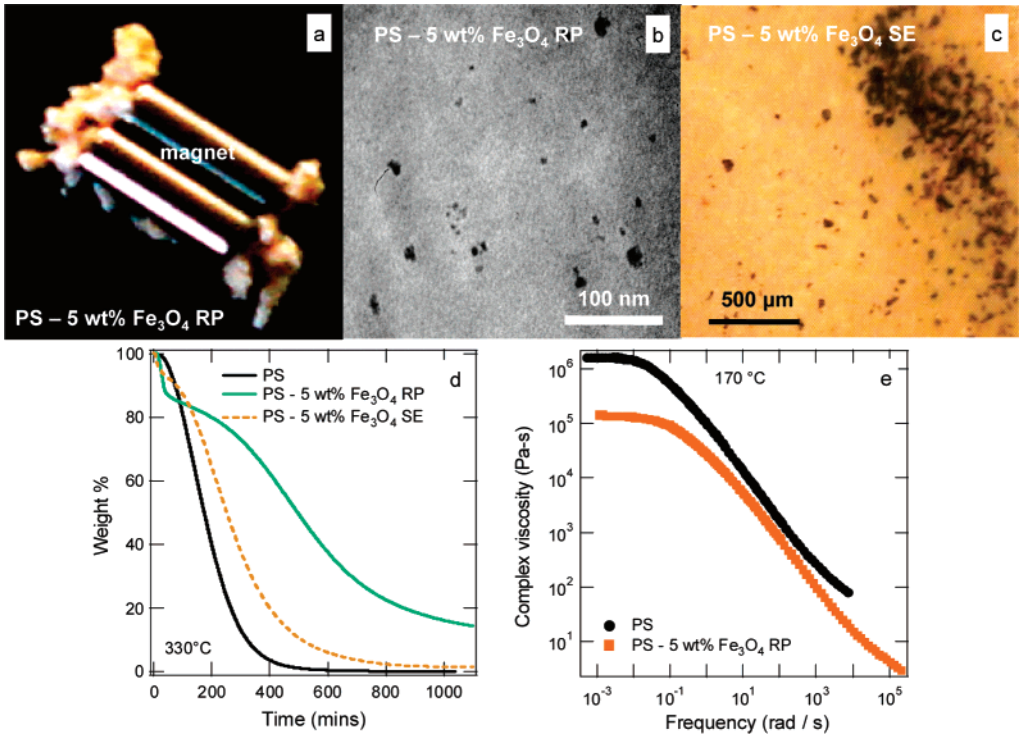

Figure 4. Multifunctional properties of magnetite nanocomposites. (a) Polystyrene is slightly colored by the dispersed magnetite nanoparticles which also cause the sample to be attracted to a permanent magnet. (b) A TEM micrograph showing good nanoparticle dispersion based on the rapid precipitation (RP) technique for mixing. On the basis of the volume fraction (∼0.01) and sample thickness, there should be ∼50 nanoparticles in this figure, which is found true. (c) Nanoparticle−polystyrene blends developed through solvent evaporation (SE) produce large phase-separated domains. (d) Also, as shown for the fullerene nanoparticles, the magnetite nanoparticles at 5 wt % decrease the rate of thermal degradation and reduce the melt viscosity at all frequencies (e). The rapidly precipitated blend (PS−5 wt % Fe_3O_4 RP) reduces the degradation rate to a greater extent than the solvent evaporated (PS−5 wt % Fe_3O_4 SE). The degradation experiment was performed at 330 °C under a nitrogen atmosphere, and the melt viscosity was measured at multiple temperatures and shifted to a reference temperature of 170 °C.

for the continued viscosity decrease despite the occurrence of small crystallites in higher concentration RP blends.

Theoretical calculations illustrating viscosity reduction would be very helpful but extremely challenging due to the dual requirements of simulating entangled melts and significant numbers of nanoparticles. Our hypothesis is that the nanoparticles provide constraint release since they diffuse ∼100 times faster than predicted by the Stokes−Einstein relation.[38] Since their time scale is much shorter than the polymer molecules, they do not participate in the entanglement dynamics and so merely produce a dilution effect which translates to a viscosity reduction.

Viscoelastic materials are important in damping applications;[39] however, issues like poor thermal stability, reliability, and high weight penalty have severely affected their large-scale development. Recently, Suhr et al.[40] showed that addition of multiwalled carbon nanotubes (MWNT) to epoxy can greatly improve its mechanical damping properties.[41] This improvement in damping properties, without any detrimental effects on the polymer strength, was ascribed to the large surface to volume ratio typical of dispersed nanoscale fillers.[40]

A simple calculation indicates that though the dispersed MWNT's material used in the previous study[40] have an interfacial contact area of ∼100 m^2/g, dispersed fullerene materials at the same weight fraction have a much larger interfacial contact area of ∼1300 m^2/g and so may significantly enhance damping. This is verified in Figure 3b, where a 5-fold increase in the loss modulus (E'') of the RP fullerene−polystyrene nanocomposite is observed, without significantly affecting the elastic modulus (E'). Indeed, a slight increase in the elastic modulus occurs. We note that Suhr et al. used 50 vol % of MWNT to achieve ∼3 times enhanced damping while for the 50 wt % (∼37 vol %) fullerene nanocomposite we observe a ∼5 fold increase in the loss modulus, suggesting a similar damping performance.[34]

Improvement of the thermal degradation properties of fullerene nanocomposites is illustrated in Figure 3c, where the weight loss as a function of time is presented for both RP and SE materials. All of these samples were studied isothermally at 330 °C under a nitrogen atmosphere. It can be seen addition of fullerenes causes a significant reduction in the degradation rate of polystyrene, suggesting their usage as possible fire retardants. Other experiments under an air atmosphere also show a significant improvement in thermal stability on fullerene addition. The weight fraction of the samples remaining at the end of each experiment equals the weight fraction of fullerenes in the nanocomposites, as fullerenes do not degrade at 330 °C. Prior work[42] demonstrating nanocomposites with improved fire retardant properties typically focused on the thermal stability of nanocomposites containing graphite sheets[43] and layered silicates,[44] where the spacing between the layers is in the nanometer range. In these materials, enhanced barrier properties were related to the observed improvement in thermal stability. Barrier properties take into consideration both the thermal barrier, which reduces the polymer temperature, and mass transport barrier which makes it difficult for the degradation products to leave the composite and for oxygen to diffuse into the polymer. However, this mechanism for thermal stability may not extend to our case as unusual, increased permeability has been reported in the case of nanoparticle-filled polymers. It was seen that nanoscale, fumed silica particles when blended with poly(4-methyl-2-pentyne) simultaneously and rather surprisingly enhance both membrane permeability and selectivity for large organic molecules over small permanent gases.[33] Such an effect

Table 1. Design Strategies for Simple Multifunctional Nanocomposites[a]

parameter	parameter values for dispersion and to enhance bulk properties
method for dispersion	rapid precipitation yields better nanoparticle dispersion than solvent evaporation
polymer size (R_g)	$R_g > a$ for nanoparticle dispersion; $R_g > h$ for viscosity reduction
polymer molecular mass (M)	$M > M_c$ for viscosity reduction with nanoparticle addition; M also determines R_g
nanoparticle radius (a)	$R_g > a$ and $a > \delta$ to promote nanoparticle dispersion
nanoparticle concentration	determines the interparticle half gap, h; $R_g > h$ for viscosity reduction
nanoparticle shape	so far, only well-dispersed spherical nanoparticles have been shown to cause a viscosity decrease; the spherical shape also leads to very high interfacial contact areas, which enhances the mechanical damping of nanocomposites; elastic properties, barrier properties, electrical properties, and thermal degradation may be further enhanced by use of anisotropic nanoparticles

[a] The first requirement is to ensure that the mixing enthalpy of the nanoparticles in the polymer melt of choice is not too unfavorable. Chemistry is used to organically functionalize inorganic nanoparticles to ensure this condition, and the physical properties of brush such as its density and chain length can also be used to control mixing enthalpy. The polymer molecular mass (M), radius of gyration (R_g), and nanoparticle radius (a) are key physical factors affecting dispersion. The critical molecular mass for entanglement coupling (M_c) designates where a viscosity reduction is possible.[5,6] The average interparticle half-gap (h) is also important for a viscosity decrease to occur. Finally, dispersion may be promoted for nanoparticles whose radius is larger than the distance that van der Waals forces propagates (δ), provided their size is smaller than R_g.[4]

in our case would promote thermal degradation of the polymer by decreasing the mass transport barrier.

In more recent work, it has been postulated that the formation of a jammed network of nanofillers is essential to improving the thermal degradation properties of nanocomposites containing nanotubes and carbon black.[37] However, in our case we see significant improvements in the thermal properties coupled with a large viscosity *decrease* (Figure 3a), indicating the absence of a jammed or gel-like network of nanoparticles within the polymer melt. Indeed, the formation of a gel-like network in the case of carbon black particles would indicate their phase separation from the polymer, especially if the radius of the carbon black particles is greater than the radius of gyration of the linear polymer ($R_g < a$).[4] One intriguing possibility is that the degradation products are indeed trapped by the fullerene nanoparticles, implying a transient physical attraction between the degradation products and the fullerenes. This is similar to the dispersion mechanism we have already discussed[4] and relies on the thermodynamic interaction between the oligomeric degradation products and the nanoparticles until the oligomers become so small that it is entropically favorable for them to be in the gaseous phase. This aspect of the degradation results is a subject of further experimental analysis.

The electrical conductivity of the fullerene−polystyrene nanocomposites is presented in Figure 3d. As has been seen before with the addition of nanoscale fillers to thermoplastics[45,46] and polymer electrolytes,[47] RP fullerene nanocomposites have increased conductivity as compared to pure polystyrene (Figure 3d). It is interesting that this increase in conductivity, even though small, is much greater than Maxwell's predicted increase[48] for an infinitely conductive spherical filler. This unusual increase in conductivity is expected to be related to the small interparticle gap ($2h$) in the nanocomposite. This small gap would allow charge transfer by electron hopping between electronegative fullerenes[49,50] (if they are close enough) and may even allow for ballistic electron transfer.[51] In comparison, a nanocomposite prepared by solvent evaporation has a lower conductivity than neat polystyrene (Figure 3d), with the dominant contributing factor being the absence of a network of fullerenes with small interparticle gaps.

Taken together, the data presented above demonstrate that fullerene nanocomposites produced by rapid precipitation are truly multifunctional[2] with enhanced damping properties, better thermal stability, greater electrical conductivity, and a much reduced melt viscosity allowing for easier melt processing using existing industrial technologies, like injection molding and extrusion. It is also the first time that all of these improvements in bulk properties have been shown to occur simultaneously in any nanocomposite as far as we know.

4. Results and Discussion: Magnetic Nanoparticles Dispersed in Polystyrene

To determine whether RP processing and the multifunctional performance it produces can be generalized, we studied a completely different, inorganic−nanoparticle/polymer system consisting of magnetite nanoparticles in the same 393 kDa linear polystyrene. A picture of the nanocomposite prepared by rapid precipitation, attracted to a permanent magnet, is shown in Figure 4a, demonstrating that incorporation of the nanoparticles has made the nanocomposite magnetic. Again, rapid precipitation and the condition that R_g is larger than a enable good dispersion of the nanoparticles, as evidenced by the TEM image shown in Figure 4b. Image analysis shows that the nanoparticles are quite polydisperse with their radius varying between 5 and 10 nm. Note that these nanoparticles could not be dispersed in polymers with molecular mass less than ∼100 kDa, even using the rapid precipitation technique, in accord with the condition $a < R_g$ to promote dispersion.[4]

Good dispersion of the magnetic nanoparticles, at this high density, opens up a plethora of possible future applications including electromagnetic shielding, high-density memory, magnetic recording, drug delivery, and separation aids.[52−54] As was the case with fullerenes, solvent evaporation leads to large-scale phase separation (Figure 4c, note the change in the scale bar compared to Figure 4b) due to the difference in solubility between the nanoparticles and the polymer in the common solvent (benzene). The incorporation of the ferromagnetic nanoparticles using rapid precipitation also improves the thermal stability (Figure 4d) of the nanocomposite, and again the stability of the rapidly precipitated blend is better than the blend prepared by solvent evaporation. The initial, rapid weight loss for time less than 100 min is most likely due to the steric stabilizing layer on the nanoparticles leaving the system (see Experimental Methods section). Use of RP to disperse magnetite nanoparticles in entangled polystyrene melts also causes a massive reduction in the melt viscosity (Figure 4e), and we find that just 5 wt % (or ∼1 vol %) of the magnetite nanoparticles causes an ∼90% reduction in the polymer melt viscosity, which is again one of the largest viscosity decreases reported through the addition of nanoparticles.

5. Conclusion

We showed that viscosity reduction, first observed in enthalpy matched systems consisting of polystyrene nanoparticles in polystyrene, also occurs in fullerene−polystyrene and in magnetic nanoparticle−polystyrene blends, provided the blends are prepared using rapid precipitation. In both cases we found that slow evaporation leads to nanoparticle agglomeration and an absence of viscosity reduction. Moreover, property improvements occur in concert with viscosity reduction, enabling facile fabrication of multifunctional nanocomposites.

The improvement in thermal stability and the viscosity decrease seen in both fullerene−linear polystyrene blends and inorganic nanoparticle−polymer systems fabricated using rapid precipitation methods indicate that the phenomena underlying the effects are quite general and not the result of specific chemical or physical interactions, as illustrated in recent theoretical work.[55] Broad guidelines for preparation of multifunctional nanocomposites with *reduced viscosity* according to our experience may then be summarized, as shown in Table 1. Though nanocomposites may of course be produced using other design strategies, those presented in Table 1 provide a robust and general set of guidelines for the design of multifunctional nanocomposites with reduced viscosity in cases where specific interactions are subdominant.

Acknowledgment. Financial support from NSF CTS-0400840, NSF NIRT- 0506309, NSF NIRT- 0210247, and DOE DE-FG02-05ER46211 is greatly appreciated. We also thank Alicia Pastor for her help with the TEM experiments.

References and Notes

(1) Gao, F. *Mater. Today* **2004**, *7*, 50−55.
(2) Vaia, R. A.; Wagner, H. D. *Mater. Today* **2004**, *7*, 32−37.
(3) Curtin, W. A.; Sheldon, B. W. *Mater. Today* **2004**, *7*, 44−49.
(4) Mackay, M. E.; Tuteja, A.; Duxbury, P. M.; Hawker, C. J.; Horn, B. V.; Guan, Z.; Chen, G.; Krishnan, R. S. *Science* **2006**, *311*, 1740−1743.
(5) Mackay, M. E.; Dao, T. T.; Tuteja, A.; Ho, D. L.; Horn, B. V.; Kim, H.-C.; Hawker, C. J. *Nat. Mater.* **2003**, *2*, 762−766.
(6) Tuteja, A.; Mackay, M. E.; Hawker, C. J.; Horn, B. V. *Macromolecules* **2005**, *38*, 8000−8011.
(7) Sariciftci, N. S.; Smilowitz, L.; Heeger, A. J.; Wudl, F. *Science* **1992**, *258*, 1474−1477.
(8) Hoppe, H.; Sariciftci, N. S. *J. Mater. Res.* **2004**, *19*, 1924−1945.
(9) Hebard, A. F.; Rosseinsky, M. J.; Haddon, R. C.; Murphy, D. W.; Glarum, S. H.; Palstra, T. T. M.; Ramirez, A. P.; Kortan, A. R. *Nature (London)* **1991**, *350*, 600.
(10) Tanigaki, K.; Ebbesen, T. W.; Saito, S.; Mizuki, J.; Tsai, J. S.; Kubo, Y.; Kuroshima, S. *Nature (London)* **1991**, *352*, 222.
(11) Chen, B.-X.; Wilson, S. R.; Das, M.; Coughlin, D. J.; Erlanger, B. *Proc. Natl. Acad. Sci. U.S.A.* **1998**, *95*, 10809−10813.
(12) Brabec, C. J.; Dyakonov, V.; Sariciftci, N. S.; Graupner, W.; Leising, G.; Hummelen, J. C. *J. Chem. Phys.* **1998**, *109*, 1185−1195.
(13) Weng, D.; Lee, H. K.; Levon, K.; Mao, J.; Scrivens, W. A.; Stephens, E. B.; Tour, J. M. *Eur. Polym. J.* **1999**, *35*, 867−878.
(14) Lu, Z.; He, C.; Chung, T.-S. *Polymer* **2001**, *42*, 5233−5237.
(15) Martensa, T.; D'; Haenb, J.; Muntersa, T.; Beelena, Z.; Gorisb, L.; Mancab, J.; D'; Olieslaegerb, M.; Vanderzandea, D.; Scheppera, L. D.; Andriessenc, R. *Synth. Met.* **2003**, *138*, 243−247.
(16) Nakatani, A. I.; Chen, W.; Schmidt, R. G.; Gordon, G. V.; Han, C. C. *Polymer* **2001**, *42*, 3713−3722.
(17) Nakatani, A. I.; Chen, W.; Schmidt, R. G.; Gordon, G. V.; Han, C. C. *Int. J. Thermophys.* **2002**, *23*, 199−209.
(18) Sen, S.; Xie, Y. P.; Kumar, S. K.; Yang, H. C.; Bansal, A.; Ho, D. L.; Hall, L.; Hooper, J. B.; Schweizer, K. S. *Phys. Rev. Lett.* **2007**, 98, -.
(19) Balazs, A. C.; Emrick, T.; Russell, T. P. *Science* **2006**, *314*, 1107−1110.
(20) Ginzburg, V. V. *Macromolecules* **2005**, *38*, 2362−2367.
(21) Hooper, J. B.; Schweizer, K. S. *Macromolecules* **2006**, *39*, 5133−5142.
(22) He, G.; Ginzburg, V. V.; Balazs, A. C. *J. Polym. Sci., Part B: Polym. Phys.* **2006**, *44*, 2389−2403.
(23) Du, F. M.; Fischer, J. E.; Winey, K. I. *J. Polym. Sci., Part B: Polym. Phys.* **2003**, *41*, 3333−3338.
(24) Green, D. L.; Mewis, J. *Langmuir* **2006**, *22*, 9546−9553.
(25) King, S. M. Small-angle neutron scattering. In *Modern Techniques for Polymer Characterisation*; Pethrick, R. A., Dawkins, J. V., Eds. John Wiley & Sons: New York, 1999.
(26) Kopesky, E. T.; Haddad, T. S.; Cohen, R. E.; McKinley, G. H. *Macromolecules* **2004**, *37*, 8992−9004.
(27) Heiney, P. A.; Fischer, J. E.; Mcghie, A. R.; Romanow, W. J.; Denenstein, A. M.; Mccauley, J. P.; Smith, A. B.; Cox, D. E. *Phys. Rev. Lett.* **1991**, *66*, 2911−2914.
(28) Fischer, J. E.; Heiney, P. A.; Mcghie, A. R.; Romanow, W. J.; Denenstein, A. M.; Mccauley, J. P.; Smith, A. B. *Science* **1991**, *252*, 1288−1290.
(29) Cotton, J. P.; Decker, D.; Benolt, H.; Farnoux, B.; Higgins, J.; Jannink, G.; Ober, R.; Picot, C.; desCloizeaux, J. *Macromolecules* **1974**, *7*, 863−872.
(30) Flory, P. J. *Principles of Polymer Chemistry;* Cornell University Press: Ithaca, NY, 1953.
(31) Ginzburg, V.; Balazs, A. *Adv. Mater.* **2000**, *12*, 1805−1809.
(32) Ginzburg, V.; Singh, C.; Balazs, A. *Macromolecules* **2000**, *33*, 1089−1099.
(33) Merkel, T. C.; Freeman, B. D.; Spontak, R. J.; He, Z.; Pinnau, I.; Meakin, P.; Hill, A. J. *Science* **2002**, *296*, 519−522.
(34) Ferry, J. D. *Viscoelastic Properties of Polymers*, 3rd ed.; J. Wiley & Sons: New York, 1980.
(35) Krishnamoorti, R.; Ren, J.; Silva, A. S. *J. Chem. Phys.* **2001**, *114*, 4968−4973.
(36) Kharchenko, S. B.; Douglas, J. F.; Obrzut, J.; Grulke, E. A.; Migler, K. B. *Nat. Mater.* **2004**, *3*, 564−568.
(37) Kashiwagi, T.; Du, F. M.; Douglas, J. F.; Winey, K. I.; Harris, R. H.; Shields, J. R. *Nat. Mater.* **2005**, *4*, 928−933.
(38) Tuteja, A.; Mackay, M. E.; Narayanan, S.; Asokan, S.; Wong, M. S. *Nano Lett.* **2007**, *7*, 1276−1281.
(39) Biggerstaff, J. M.; Kosmatka, J. B. *J. Comp. Mater.* **1999**, *33*, 1457−1469.
(40) Suhr, J.; Koratkar, N.; Keblinski, P.; Ajayan, P. *Nat. Mater.* **2005**, *4*, 134−137.
(41) Koratkar, N.; Wei, B. Q.; Ajayan, P. M. *Adv. Mater.* **2002**, *14*, 997-+.
(42) Porter, D.; Metcalfe, E.; Thomas, M. J. K. *Fire Mater.* **2000**, *24*, 45−52.
(43) Nyden, M. R.; Gilman, J. W. *Comp. Theor. Polym. Sci.* **1997**, *7*, 191−198.
(44) Zhu, J.; Morgan, A. B.; Lamelas, F. J.; Wilkie, C. A. *Chem. Mater.* **2001**, *13*, 3774−3780.
(45) Charati, S. G.; Dibakar, D. D.; Elkovitch, M.; Ghosh, S.; Mutha, N.; Rajagopalan, S.; Shaikh, A. A. Electrically conductive compositions and method of manufacture thereof, 7,026,432, 2006.
(46) Thompson, C. M.; Herring, H. M.; Gates, T. S.; Connell, J. W. *Comput. Sci. Technol.* **2003**, *63*, 1591−1598.
(47) Croce, F.; Appetecchi, G. B.; Persi, L.; Scrosati, B. *Nature (London)* **1998**, *394*, 456−458.
(48) Maxwell, J. C. *A Treatise on Electricity and Magnetism*, 2nd ed.; Oxford University Press: Cambridge, 1904.
(49) Arici, E.; Sariciftci, N. S.; Meissner, D. Hybrid Solar Cells. In *Encyclopedia of Nanoscience and Nanotechnology*; Nalwa, H. S., Ed.; American Scientific Publishers: Valencia, 2004.
(50) Ounaies, Z.; Park, C.; Wise, K. E.; Siochi, E. J.; Harrison, J. S. *Compos. Sci. Technol.* **2003**, *63*, 1637−1646.
(51) Keblinski, P.; Phillpot, S. R.; Choi, S. U. S.; Eastman, J. A. *Int. J. Heat Mass Transfer* **2002**, *45*, 855−863.
(52) Talbot, P.; Konn, A. M.; Brosseau, C. *J. Magn. Magn. Mater.* **2002**, *249*, 481−485.
(53) Ditsch, A.; Laibinis, P. E.; Wang, D. I. C.; Hatton, T. A. *Langmuir* **2005**, *21*, 6006−6018.
(54) Ahmed, S. R.; Ogale, S. B.; Kofinas, P. *IEEE Trans. Magn.* **2003**, *39*, 2198−2200.
(55) Curro, J. G.; Frischknecht, A. L. Manuscript in preparation.

MA071313I